Study of The Performance of A Cylindrical Flow-Through Electro-Fenton Reactor Using Different Arrangements of Carbon Felt Electrodes: Degradation of Amoxicillin In Aqueous Solution

Josué Daniel García-Espinoza
CIDETEQ: Centro de Investigacion y Desarrollo Tecnologico en Electroquimica SC
Irma Robles
CIDETEQ: Centro de Investigacion y Desarrollo Tecnologico en Electroquimica SC
Alfonso Durán-Moreno
UNAM Facultad de Quimica: Universidad Nacional Autonoma de Mexico Facultad de Quimica
Luis A. Godinez (lgodinez@cideteq.mx)
CIDETEQ: Centro de Investigacion y Desarrollo Tecnologico en Electroquimica SC
https://orcid.org/0000-0002-4136-3858

Research Article

Keywords: amoxicillin, carbon felt, disinfection, electro-Fenton

Posted Date: August 13th, 2021

DOI: https://doi.org/10.21203/rs.3.rs-589843/v1

Study of the performance of a cylindrical flow-through electro-Fenton reactor using different arrangements of carbon felt electrodes: degradation of amoxicillin in aqueous solution

Josué Daniel García-Espinoza[1], Irma Robles[1], Alfonso Durán-Moreno[2], Luis A. Godínez[1,3 *]

[1] Centro de Investigación y Desarrollo Tecnológico en Electroquímica, Parque Tecnológico Querétaro Sanfandila, 76703, Pedro Escobedo, Querétaro, México.
[2] Facultad de Química, Universidad Nacional Autónoma de México, CDMX, México.
[3] On leave to: Facultad de Química, Universidad Autónoma de Querétaro, Querétaro, México.

* Corresponding author: Luis A. Godínez, lgodinez@cideteq.mx

Keywords: amoxicillin, carbon felt, disinfection, electro-Fenton

Abstract

In this work, a cylindrical flow-through electro-Fenton reactor integrated by graphite felt electrodes and Fe(II) loaded resin was evaluated for the production of the Fenton reaction mixture and for the degradation of amoxicillin (AMX) containing aqueous solutions. First, the influence of several factors such as treatment time, current intensity, flow rate and electrode position were investigated for the electrogeneration of H_2O_2 and the energetic consumption by means of a factorial design methodology using a 2^4 factorial matrix. Electric current and treatment time were found to be the pivotal parameters influencing the H_2O_2 production with respective contributions of 40.2% and 26.9%. The flow rate had low influence on the responses, however, 500 mL min^{-1} (with an average residence time of 1.09 min obtained in the residence time distribution analysis) allowed to obtain a better performance due to the high mass transport to and from the electrodes. As expected, polarization was also found to play an important role, since for cathode-to-anode flow direction, lower H_2O_2 concentrations were determined when compared with anode-to-cathode flow arrangement, indicating that part of the H_2O_2 produced in the cathode could be destroyed at the anode. A fluorescence study of hydroxyl radical production on the other hand, showed that higher yields were obtained using an anode-to-cathode flow direction (up to 3.88 µM), when compared with experiments carried out using a cathode-to-anode flow direction (3.11 µM). The removal of a commercial formulation of the antibiotic amoxicillin (AMX) was evaluated in terms of total organic carbon, achieving up to 57.9 % and 38.63% of the pollutant mineralization using synthetic and real sanitary wastewater spiked, respectively. Finally, the efficiency of the process on the inactivation of fecal coliforms in sanitary wastewater samples was assessed, reducing 90% of the bacterium after 5 min of electrolysis.

Introduction

Electrochemical advanced oxidation processes (EAOPs) constitute an attractive approach to treat wastewater effluents contaminated with persistent pollutants. These processes are characterized by the use of hydroxyl radicals (•OH) which are strong oxidant species capable of attacking a wide variety of organic contaminants (E°= 2.8 V *vs.* standard hydrogen electrode, SHE) (Comninellis 1994; Brillas et al. 2009; Brillas 2020). Among the different EAOPs, the so-called electro-Fenton processes are quite promising since they are based on the *in situ* electro-generation of H_2O_2 by means of the 2e-reduction of dissolved oxygen at a suitable cathode material under acid or alkaline conditions (see Eq. (1) -(2)), and in the presence of an iron promoter as shown in Eq. (3) (Salmerón et al. 2021).

$$O_2 + 2H^+ + 2e^- \rightarrow H_2O_2 \qquad (1)$$

$$2H_2O + O_2 + 2e^- \rightarrow H_2O_2 + 2OH^- \qquad (2)$$

$$H_2O_2 + Fe^{2+} \rightarrow Fe^{2+} + {}^{\bullet}OH + OH^- \qquad (3)$$

Since the electro-Fenton process involves electrochemical reactions, its performance is limited by the mass transport of oxygen and the pollutant species to the electrode surface and therefore it nis closely related to the reactor design (Garcia-Segura et al. 2020). Over the last years, the design of most of the continuous-flow electro-Fenton reactors has focused on the flow-by configuration, where the pollutant containing effluent flows parallel to the anode and cathode surfaces (Zhou et al. 2017). In these systems, convection becomes negligible near the electrode-solution interface and therefore, in order to reduce the mass transport limitations of the conventional flow-by reactors, it is important to incorporate fluid mixer promotors such as mechanical agitators or pumps.

In this way, flow-through electro-Fenton reactors stand out as an attractive option to overcome these weaknesses since the solution flows through porous anode and cathode electrodes, increasing mass transport events that result in improved electrochemical conversion, current efficiency and reduced energy consumption (Zhou et al. 2017). In flow-through electro-Fenton reactors, 3D porous electrodes have shown good yields in the abetment of several pollutants (Jiao et al. 2020; Yu et al. 2020) and among the electrodes employed, carbonaceous materials, such as graphite felt, stand out as desirable electrodes because of their stability, electric conductivity, high surface area, chemical resistance, efficient cathodic regeneration of Fe(II) as well as its inherent filtration characteristics (Brillas et al. 2009; Panizza and Oturan 2011; Zhou et al. 2012, 2014, 2017; Petrucci et al. 2016).

Due to these features, the performance of flow-through electro-Fenton reactors has been extensively reported. For instance, Ren et al., (2016) studied the degradation of tartrazine in a vertical-flow electro-Fenton reactor, made up 10 cell compartments using a PbO_2 anode and a modified graphite felt mesh cathode. Those authors reported the complete abatement of the pollutant and 61% of total organic carbon (TOC) removal at pH 3, using a voltage of 4.0 V, a flow rate of 40 mL min^{-1}, and a concentration of 0.4 mM Fe(II) (Ren et al. 2016). In a subsequent study, Ren et al. (2020) also reported the treatment of real domestic sewage using a stacked flow-through electro-Fenton reactor equipped with modified graphite felt cathodes and DSA mesh anodes. Applying 2.5 V and using adding 0.4 mM Fe(II) these authors obtained a bacterium inactivation value of log 3.34–3.46 and efficient removals of COD, N-NH_3 and total phosphorus (Ren et al. 2020). Also, Chai et al. (2021) evaluated a coupled system of flow-through electro-Fenton and electrosorption processes for the treatment of high-salinity organic wastewater using iron, Ti and activated carbon felt electrodes. In this work, the authors achieved chemical oxygen demand (COD) removals, total nitrogen and salinity of 96.5, 98.2, and 46.2%, respectively (Chai et al. 2021). The modification of activated carbon fibers coupled to a DSA anode in a flow-through electro-Fenton process for orange II dye abetment has also been reported by Jiao et al., (2020) (Jiao et al. 2020).

As it can be seen, from these and other reports, good yields on pollutant removal are obtained using flow-through electro-Fenton configurations. However, the use of anodes such as iron, PbO_2 or DSA and the need to add Fe(II) as the Fenton mixture promoter, limit the use of these reactors in large-scale applications and in this context, flow-through electro-Fenton reactors equipped with electrodes made of affordable carbonaceous materials and where the Fe(II) is provided and retained by an ion exchange resin has also been reported by our research group (García-Espinoza et al. 2019; Robles et al. 2020).

In spite of the interest in 3D and flow-through reactors, there is still a severe lack on the understanding of reactor configuration effects since most electrochemical publications focus on novel electrode materials rather than on recognizing the significant influences of mass transport on pollutant degradation (Garcia-Segura et al. 2020). In this way, the flow direction of the solution is an important operational variable in flow-through reactors because it can control the overall performance of the process. This is the case of the electrochemical elimination of N-NH_4, in which by arranging an anode-to-cathode flow is possible to achieve its removal and obtain safe N_2, since in the anode, the oxidation of N-NH_4 to NO_2^- and NO_3^- is achieved, prior to its subsequent reduction to N_2 in the

cathode. These sequence of reactions are not obtained in the cathode-to-anode flow configuration (Heck et al. 2019; Garcia-Segura et al. 2020; Ren et al. 2020).

The performance of the electro-Fenton process has also been tested for the degradation of biorecalcitrant pollutants (Komtchou et al. 2015; García-Espinoza et al. 2019; Castillo-Monroy et al. 2020; Droguett et al. 2020; Puga et al. 2021). Among them, the elimination from aquatic media of antibiotic compounds such as amoxicillin (AMX) is relevant since this a pharmaceutical compound that is widely used in human and veterinary medicine (aus der Beek et al. 2016). As a consequence, AMX is frequently detected in the environment since 60 to 90% of the substance is excreted without alteration (Mompelat et al. 2009). Due to its physicochemical proprieties such as low $LogK_{ow}$ value, low volatility, high stability, high polarity and complex chemical structure (Table 1), the AMX is a persistent compound which may result in eco-toxicological effects and human health affectations (Jones et al. 2002) and therefore, AMX is one of the 19 compounds in the *watch list* of substances being monitored by the European Union (Commission Implementing Decision (EU) 2015).

Table 1. Physicochemical properties of the amoxicillin.

Pharmaceutical group	Aminopenicillin antibiotic
Molecular formula	$C_{16}H_{19}N_3O_5S$
CAS	26787-78-0
Chemical structure	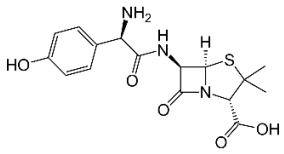
Molecular mass (g mol^{-1})	365.4
Water solubility (mg L^{-1})	$3.43x10^3$
pKa	3.2, 11.7
$LogK_{OW}$	0.87
Henry's law constant (atm m^3mol^{-1})	$2.49X10^{-21}$

pKa: acid dissociation constant; $logK_{ow}$: octanol–water partition coefficient

In the context of the interest to develop efficient EAOPs for the degradation of commercial formulations of biorecalcitrant compounds (Murillo-Sierra et al. 2018; de Matos et al. 2020; Carrera-Cevallos et al. 2021), the aim of this work was to evaluate the performance on the degradation of AMX of a flow-through electro-Fenton reactor equipped with carbon felt electrodes. First, residence time distribution was investigated. Later, the capability of the electrochemical reactor to generate H_2O_2 was evaluated at different current intensities, recirculation flow, treatment time and position of the

electrodes, also considering the energetic consumption. Afterwards, the process effectivity for AMX abatement was evaluated under different experimental conditions and the process was also tested for the inactivation of fecal coliforms using real sanitary wastewater.

Materials and methods

Chemicals and solutions

While coumarin and cerium sulphate (IV) was purchased from Sigma-Aldrich, H_2SO_4, NaCl and Na_2SO_4 were reagent grade supplied by J.T. Baker. A commercial formulation of the antibiotic AMX (AMSA, Mexico) in capsule presentation of 500 mg was employed. For the determination of H_2O_2, solutions were prepared using demineralized water dissolving 0.05 M of Na_2SO_4 as supporting electrolyte. Using this electrolyte, solutions of coumarin (0.4 mM) and AMX (0.27 mM) were used. Samples of real sanitary wastewater pretreated by biological processes were also used (chemical oxygen demand, COD: 45.6±16, pH 7.7±0.2, conductivity: 0.9 ±0.04 mS cm^{-1}). While the pH of all solutions was 7.0 ± 0.5, the electric conductivity of the Na_2SO_4 electrolyte and the sanitary wastewater were 8.8 ± 0.4 and 0.8 ± 0.2 mS cm^{-1}, respectively.

Electro-Fenton Reactor

The treatment was carried out using a three-compartment cylindrical reactor (horizontally oriented) made of Nylamid. The central compartment with a 141 cm^3volume, and two identical sections were coupled on the up- and low-ends of the middle section using stainless steel screws (Fig. 1a). The experimental set-up consisted of the reactor equipped with a power source, a peristaltic pump, a recirculation tank and an oxygen concentrator (Fig. 1b). Carbon cloth circular pieces (28 cm^2 effective area, 0.6 mm thickness, 0.5 Ω in^2 electrical resistivity) served as electrical contacts for cylindrical carbon felt electrodes (6 cm diameter, 2.35 cm length), positioned between the compartments (Fig. 1c and 1d). For the electro-Fenton assays, while in the compartment next to the cathode a cation exchange resin containing Fe(II) was placed, the same amount of a Na^+-activated cation exchange resin was located in the compartment next to the anode (Fig. 1e). As can be seen in Fig. 1a, the reactor was fed in such a way that the pollutant solution passed through the three sections the reactor; that is, across the resin compartments and the polarized cloth and carbon felt electrodes, flowing towards a receiving tank where the effluent solution was mixed with the influent solution and from

where the solution is pumped by means of a peristaltic pump. Oxygen was fed to the solution using an oxygen concentrator (AEROUS, CleanWater Tech.) and a Venturi jet aerator in the inlet line at a constant flow rate of 250 mL min^{-1}. Electrical current was applied using a power supply (Keithley 2400). All assays were conducted in batch mode under galvanostatic conditions at room temperature (25 °C). The working volume of the electrochemical system was 0.5 L.

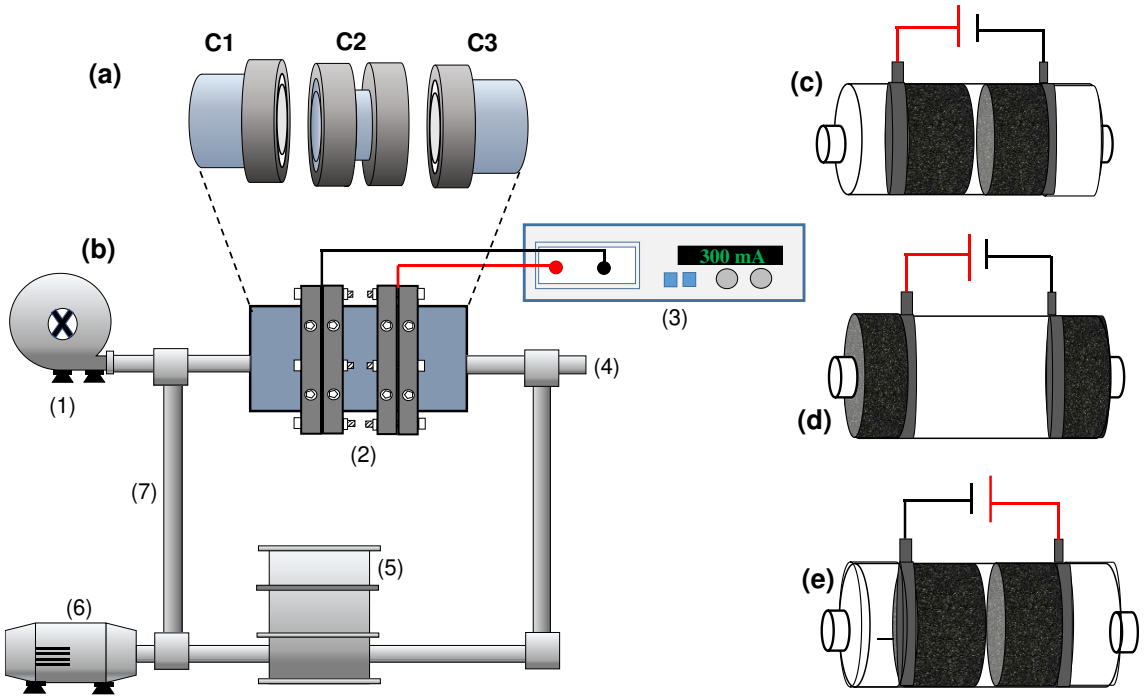

Fig. 1. (a) Electrochemical reactor scheme where C*i* represents the different compartments and (b) schematic diagram of the experimental set-up. (1) oxygen concentrator, (2) electrochemical reactor, (3) power supply, (4) sample point, (5) recirculation tank, (6) peristaltic pump, (7) recirculation pipe; (c) electrodes placed in the center arrangement, (d) electrodes placed in the extremes arrangement, (e) configuration where resin is placed in C*1* and C*3* compartments.

Experimental set-up and methods

Residence time distribution (RTD) was obtained from a tracer test which was conducted using the pulse injection method. In this experiment, a concentrated solution of NaCl was instantly introduced to the inlet line of the reactor and total dissolved solids (TDS) were measured every 5 s at the outlet of the reactor. The normalized residence time

192 distribution function (*E(t)*) and the average residence time (μ) after the pulse tracer input
193 was obtained using Eq. (4) and (5) respectively (Martin-Dominguez et al. 2005):

194 $$E(t) = \frac{C(t)}{\int_0^\infty C(t)dt} \qquad (4)$$

195 $$\mu = \frac{\int_0^\infty t\, C(t)dt}{\int_0^\infty C(t)dt} \qquad (5)$$

196 In these equations, *C(t)* corresponds to the tracer concentration evolution at the reactor
197 exit and *t* is the time. Later, a full 2^4 factorial design (FD) was used to investigate the
198 effect of the factors and their interactions on the electrogeneration of H_2O_2 and in the
199 energetic consumption of the process. From the FD an empirical linear model is obtained
200 (see Eq. (6)):

201 $$Y_j = \beta_0 + \sum \beta_i X_i \qquad (6)$$

202 Here, Y_j is the response variable, X_i is the independent variable and β_o, and β_i,
203 correspond to the constant and the linear model coefficients, respectively (Aquino et al.
204 2013). Four independent factors were studied: electrolysis time (X_1), current intensity
205 (X_2), recirculation flow (X_3) and the position of the electrodes (X_4). Three of these
206 variables were quantitative factors (X_1, X_2 and X_3) and one corresponded to a categorical
207 factor (X_4). Sixteen assays were required for the FD. Experimental data were analyzed
208 using the Design Expert® program software (Design Expert 7, Stat-Ease Inc.,
209 Minneapolis). The DF was developed within the range of the independent variables
210 according to Table 2. Once the conditions that maximize the H_2O_2 electrogeneration
211 were determined, the percentage of current efficiency (ϕ) for the production of H_2O_2 was
212 computed using Eq. (7), where *n* is the number of transferred electrons (2) to produce
213 H_2O_2 via oxygen reduction, *F* is the Faraday constant (96 485 C mol^{-1}), C_{H2O2} is the H_2O_2
214 concentration (in g L^{-1}), V is the volume of the solution (in L), M_{H2O2} is the molecular
215 weight of H_2O_2 (34.01 g mol^{-1}), *I* is the applied current (in A) and t is the treatment time
216 (in s) (Ma et al. 2019).

217 $$\phi = \frac{nFC_{H2O2}V}{M_{H2O2}It}100 \qquad (7)$$

218 The energetic consumption per cubic meter of treated water (EC) was calculated using
219 Eq. (8) (Brillas and Martínez-Huitle 2015).

220 $$E_c\left(\frac{kWh}{m^3}\right) = \frac{V\, I\, t}{Vol\ 1000} \qquad (8)$$

where *V*, *A*, *t* and *Vol* correspond to the voltage (V), current (A), time (h) and the volume of treated water (m^3), respectively. It is important to note that the EC values obtained only take into account the electricity used in the electrolysis assays, disregarding the energy required to pump the solutions and that consumed in the oxygen concentrator.

Table 2. Range and codification of independent variables (X_i).

		Experimental range	
X_i	Variable	Min. value (-)	Max. value (+)
X_1	Electrolysis time (min)	15	30
x_2	Current intensity (mA)	150	300
X_3	Recycling flow rate (mL min^{-1})	375	500
X_4	Electrodes position	Center, C*2*	Extremes, C*1* and C*3*

Analytical methods

Cerium sulfate (IV) dissolved in an acid solution (H_2SO_4) with phenanthroline as indicator, was prepared and used along with a calibration curve previously constructed, to quantitatively determine the concentration of H_2O_2 using a volumetric redox titration method (Daghrir et al. 2013; Komtchou et al. 2015). Assessment of •OH radical production was carried out by measuring the generation of the fluorescent 7-hydroxicoumarin (7-HC) that results from the selective hydroxylation reaction of coumarin with the •OH electro-generated species. The wavelengths of excitation (λ_{ex}) and emission (λ_{em}) corresponded to 340 and 456 nm, respectively. Both excitation and emission slits were fixed at 5 nm. The concentration of •OH ($C_{\bullet OH}$, in µM) was determined by means of Eq. (9) which considers that 29% of all •OH radicals are trapped by coumarin to produce 7-HC (Tokumura et al. 2011). This equation also considers that 2 mol of •OH radicals react with 1 mol of coumarin to produce 1 mol 7-HC. Since the slope of the calibration curve, $C_{7\text{-HC}}$, corresponds to the concentration of 7-HC, then $C_{\bullet OH}$ can be obtained from the fluorescence intensity at 456 nm, FI_{456}.

$$C_{\bullet OH} = \left(\frac{2}{0.29}\right) C_{7-HC} = 23.45 \times 10^{-3}\ FI_{456} \qquad (9)$$

The removal of AMX on the other hand, was determined from the TOC assessment. While spectrophotometric tests were carried out using a DR600 HACH apparatus and the TOC measurements utilizing a Shimadzu TOC LCSN equipment, fluorescence measurements were performed using a Cary Eclipse Agilent spectrophotometer. pH, TDS and dissolved oxygen concentration were measured employing a Thermo Scientific

potentiometer model Orion Versa Star Pro. COD and nitrate ion (NO_3^-) concentrations were determined employing HACH reagents.

Results

Hydraulic characterization

As it was previously mentioned, he residence time distribution (RTD) was used to investigate the hydraulic characteristics of the flow-through electro-Fenton reactor under study. In a pulse, an amount of tracer is suddenly injected in one shot into the feed-stream entering the reactor. The outlet concentration is then measured as a function of time. Fig. 2 shows the obtained RTD curves at two different flow rates and using the reactor with the electrodes placed in the center (see Fig. 1c) and without the application of current.

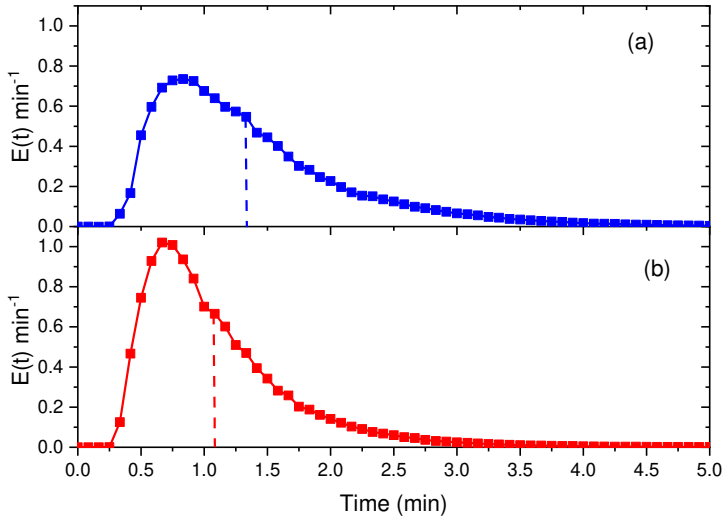

Fig. 2. RTD curves at flow rates of (a) 375 and (b) 500 mL min^{-1}. Dotted lines represent the average residence time.

The calculated average residence time under both experimental conditions corresponded to 1.37 and 1.09 min at 375 and 500 mL min^{-1}, respectively (see dotted lines in Fig. 2); which are shorter that the theoretical retention times (1.6 and 1.2 min for 375 and 500 mL min^{-1} flow rate, respectively). This reflects the fact of the porous carbon felt electrodes occupying part of the effective volume of the reactor, thus shortening the time needed for the solution to reach the outlet. Furthermore, the parabolic shape of the curves means that there is no by-pass effects in the reactor (Monteil et al. 2021), however the asymmetric shape of the tails in the curves reflects the presence of stagnant zones

(Haoran et al. 2013). At the highest flow rate, a higher and thinner peak can be observed when compared with the one obtained at the lower flow rate. This observation suggests that by increasing the flow rate it is possible to obtain a plug flow behavior and by reducing the flow rate the system behaves as a continuous-stirred tank reactor (Monteil et al. 2021). To further evaluate the effect of the flow rate on the generation of H_2O_2 for the proposed flow-through reactor, the FD study was carried out.

Effect of operational parameters

The factorial design matrix, experimental and predicted data for the H_2O_2 generated in anode-to-cathode flow direction and the calculated energy consumption are presented in Table 3. The empirical relationship between the responses and variables are expressed by the polynomial Eqs. (10)-(11).

$$Y_{H2O2} = 10.54 + 1.40X_1 + 1.71X_2 + 0.68X_3 - 1.03X_4 + 8.5x10^{-3}X_1X_2 + 0.25X_1X_3 + 0.46X_1X_4 + 0.37X_2X_3 - 0.66X_2X_4 + 0.20X_3X_4 \quad (10)$$

$$Y_{EC} = 2.26 + 0.76X_1 + 1.15X_2 - 0.22X_3 + 0.23X_4 + 0.39X_1X_2 - 0.080X_1X_3 + 0.090X_1X_4 - 0.18X_2X_3 + 0.11X_2X_4 + 0.11X_3X_4 \quad (11)$$

Table 3. Experimental factorial matrix and experimental results.

	Experimental design								H_2O_2 (mg L^{-1})		EC (kWh m^{-3})	
Exp.	X_1	X_2	X_3	X_4	Electrolysis time (min)	Current intensity (mA)	Recycling flow rate (mL min^{-1})	Electrodes position	Actual value	Predicted value	Actual value	Predicted value
1	-1	-1	-1	-1	15	150	375	Center	8.30	8.41	0.68	0.77
2	-1	1	-1	-1	30	150	375	Center	9.40	9.77	1.37	1.49
3	-1	-1	1	-1	15	300	375	Center	12.75	12.39	2.42	2.43
4	-1	1	1	-1	30	300	375	Center	13.92	13.79	4.95	4.71
5	1	-1	-1	-1	15	150	500	Center	8.50	8.12	0.64	0.63
6	1	1	-1	-1	30	150	500	Center	10.60	10.48	1.25	1.03
7	1	-1	1	-1	15	300	500	Center	13.00	13.59	1.68	1.58
8	1	1	1	-1	30	300	500	Center	16.10	15.99	3.21	3.54
9	-1	-1	-1	1	15	150	375	Extremes	6.30	6.34	0.86	0.63
10	-1	1	-1	1	30	150	375	Extremes	10.10	9.54	1.71	1.72
11	-1	-1	1	1	15	300	375	Extremes	7.50	7.69	2.60	2.71
12	-1	1	1	1	30	300	375	Extremes	10.60	10.94	5.25	5.35
13	1	-1	-1	1	15	150	500	Extremes	6.70	6.84	0.77	0.92
14	1	1	-1	1	30	150	500	Extremes	10.70	11.05	1.61	1.68

15	1	-1	1	1	15	300	500	Extremes	10.10	9.68	2.33	2.29
16	1	1	1	1	30	300	500	Extremes	14.04	13.93	4.80	4.61

The coefficient R^2, is defined as the ratio of the explained to the total variation and is a measure of the degree of fitting. For a good fit, R^2 should be at least 0.80 (Fu et al. 2007). The obtained R^2 (of 0.9871 for H_2O_2 generation and 0.9891 for energetic consumption) can be seen to be high for both responses, reflecting that the model describes reasonably well the process performance. This was also confirmed by the adjusted determination coefficients (adj-R^2) characterized by the values of 0.9614 and 0.9674 for H_2O_2 production and energetic consumption, respectively. Analysis of variance (ANOVA) of the results was also performed to evaluate the significancy of the models (Table 1-S and 2-S). The comparison of the actual and predicted values for H_2O_2 electrogeneration and energetic consumption indicate that as expected, the highest yields of H_2O_2 production and energetic consumption are reached when applying the maximum current and treatment time (Fig. 1-S).

Fig. 3a on the other hand, shows the values of the effects of the independent factors. As can be observed from inspection of this figure, H_2O_2 production, treatment time, current intensity and recycling flow show a positive effect when their values are high (b_{1H2O2}=1.40, b_{2H2O2}=1.71, b_{3H2O2}=0.68). The position of the electrodes on the other hand, show a negative effect (b_{4H2O2}=-1.03), which means that the electrodes positioned in the center allow to obtain a higher H_2O_2 concentration when compared to an arrangement in which the electrodes are located in the extreme positions of the reactor. In this way, while energetic consumption, treatment time, current intensity and position of the electrodes show a positive effect (b_{1EC}=0.76, b_{2EC}=1.15, b_{4EC}=0.23), the recirculation flow is characterized a negative effect on the response (b_{3EC}=-0.22). This means that at high flows, the energetic consumption is reduced because mass transfer to electrodes is favored; a fact that also decreases the potential difference. In order to get further insight from the experimental data; the percentage effect of each factor and their interactions on the responses were calculated using Eq. (12):

$$P_i = \left(\frac{b_i^2}{\sum_{i=1}^{k} b_i^2}\right) 100 \quad (i \neq 0) \qquad (12)$$

where *Pi* is the percentage contribution of each independent factor *i*, and where b_i represents the estimation of the main effect of the factor *i*.

As depicted Fig. 3b, the contribution of the primary effects on H_2O_2 generation corresponds to 26.9%, 40.2%, 6.24% and 14.6% for electrolysis time, current, recycling

flow rate and electrodes position, respectively. For energetic consumption on the other hand, the contribution of the same variables corresponds to 26.1%, 59.3%, 2.2% and 2.5%. As shown in Fig. 3b, the applied current is the factor with the highest contribution for both responses, followed by treatment time. The preponderant significance of current and treatment time lies in the fact that both parameters are strongly related with the amount of electric charge entering the reactor, that is, a higher number of $2e^-$ oxygen reduction events that result in the electrogeneration of H_2O_2. Similar results have been reported for the performance of EAOPs (Zaviska et al. 2011, 2012; Daghrir et al. 2014; García-Espinoza et al. 2016, 2018).

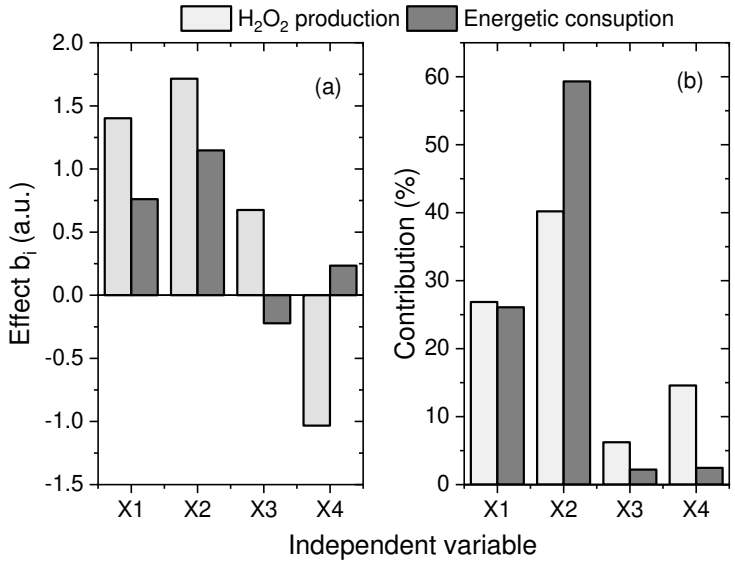

Fig. 3. (a) Effect of independent and (b) standardized factors on H_2O_2 electrogeneration and energetic consumption (X_1: time; X_2: current; X_3: recycling flow; X_4: electrodes position).

Assuming that the maximum concentration of H_2O_2 corresponds to the optimal reactor´s performance, the best operating conditions are: 30 min of electrolysis at 300 mA, 500 mL min^{-1} as recycling flow rate and arranging the electrodes in the central compartment of the reactor. Under these optimized conditions, the predicted electrogenerated H_2O_2 concentration proposed by the model corresponds to 15.99 mg L^{-1}, a value which is quite close to the experimentally obtained one (16.10 mg L^{-1}).

Fig. 4a shows the concentration of H_2O_2 on time in the anode-to-cathode flow direction under oxygen and air saturation conditions. As expected, an oxygen concentration increase allows to obtain higher yields (2.72 times more) when compared to the values achieved using air (the corresponding concentration of oxygen in the solution is 30 mgO_2 L^{-1} under oxygen saturation *vs.* 7.5 mgO_2 L^{-1} at air saturation). It is interesting to note

346 that in the cathode-to-anode flow direction arrangement under oxygen saturation
347 conditions, lower H_2O_2 concentrations were obtained when compared to the anode-to-
348 cathode set-up (16.1 and 6.1 mg L^{-1}, respectively). This observation suggest that 62% of
349 H_2O_2 produced in the cathode is consumed at the anode in this arrangement as indicated
350 by Eq. (13):

351 $$H_2O_2 + OH^- \rightarrow OH_2^{\bullet} + H_2O + e^- \qquad (13)$$

352 Similar H_2O_2 concentration values were obtained by (Zhang et al. 2021), who achieved
353 up to 17.68 mg L^{-1} at pH 3 after 120 min of electrolysis using a reticular stainless-steel
354 cathode and a DSA anode.

355 Current efficiencies for H_2O_2 generation were also determined and the resulting data is
356 shown in Fig. 4b. Inspection of the experimental curves reveals that as expected, the
357 current efficiencies are higher in the cathode-to-anode flow direction and in the presence
358 of pure oxygen.

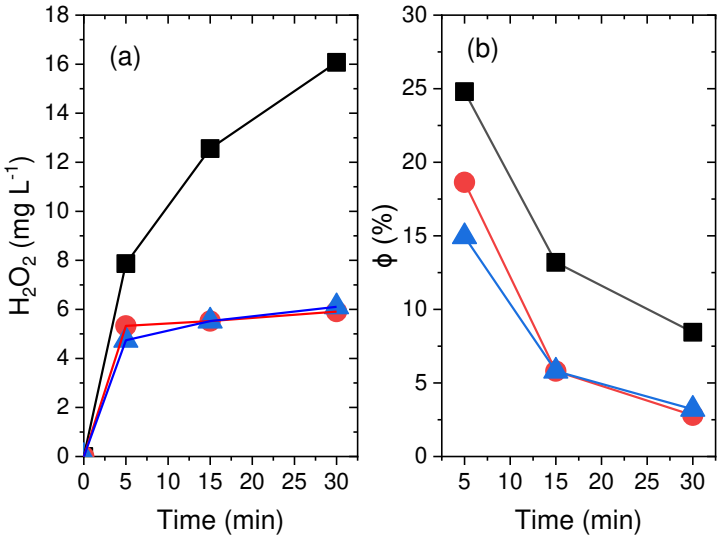

359

360 **Fig. 4.** (a) Concentration of electrogenerated H_2O_2 and (b) current efficiency. Black ■:
361 anode-to-cathode flow configuration with oxygen saturation, red •: anode-to-cathode flow
362 arrangement with air saturation, blue ▲: cathode-to-anode flow set-up with oxygen
363 saturation. Conditions: 300 mA, 0.05 M Na_2SO_4 electrolyte, pH 7, 500 mL min^{-1}
364 recirculation flow.

365

366 **Assessment of ˙OH production**

Once the experimental conditions that promote the best H_2O_2 generation were obtained, the production of ·OH was evaluated. Fig. 5 shows the fluorescence intensity and the obtained ·OH concentration. Inspection of the experimental data reveals that in the cathode-to-anode flow direction arrangement, the electro-Fenton process allows to obtain up to 132 units of fluorescence (3.11 µM of ·OH) at 5 min of electrolysis, which represents a lower production of the radical when compared with the one obtained in the anode-to-cathode flow direction set-up (up to 165 units of fluorescence, 3.88 µM of ·OH). The higher yields of the anode-to-cathode configuration can be related with the fact that the washed Fe(II) from the resin in C*1* interacts with the electrogenerated H_2O_2 in the cathode positioned after the anode, near to the outlet of the reactor. Therefore, the residual H_2O_2 in Fig. 4a promotes the production of ·OH directly in the sample point. On the other hand, the ·OH obtained in the cathode-to-anode flow direction configuration is slightly lower when compared with the aforementioned configuration. In this way, higher ·OH concentration is expected within the reactor since Fe(II) ions react directly with the electrogenerated H_2O_2 in the electrode placed at the reactor´s inlet. In the absence of Fe(II) (see Fig. 5c and 5d), the ·OH concentration is considerably smaller. The electrochemical oxidation process with the addition of air in cathode-to-anode flow direction on the other hand, allowed to obtain up to 18.2 units of fluorescence (0.42 µM of ·OH) and as expected, this value increases with the addition of pure oxygen (21.0 units of fluorescence, 0.49 µM of ·OH). In both cases, ·OH generation can be related to the monoelectronic reduction of H_2O_2 according the Eq. (14):

$$H_2O_2 + e^- \rightarrow \bullet OH + OH^- \qquad (14)$$

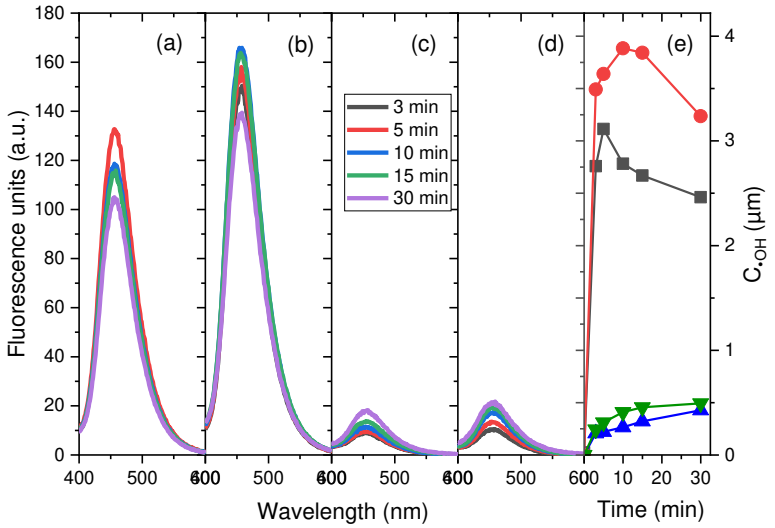

Fig. 5. Fluorescence intensity and •OH concentration in an: (a) Electro-Fenton process, cathode-to-anode arrangement, (b) anode-to-cathode flow configuration, (c) electrochemical oxidation process cathode-to-anode flow set-up with air saturation, (d) electrochemical oxidation process cathode-to-anode flow configuration with oxygen saturation, (e) •OH concentration under the different experimental conditions, determined at 456 nm (black ■: conditions of (a), red •: conditions of (b), blue ▲: conditions of (c), green ▼: conditions of (d)). 300 mA, 0.4 mM of coumarin in 0.05 M Na_2SO_4 electrolyte, pH 7, 500 mL min^{-1} recirculation flow rate.

AMX degradation

The effectiveness of the electro-Fenton process was also evaluated in terms of the mineralization of AMX. To clarify the role the processes that take place within the system, different experimental conditions were evaluated; namely: adsorption (without current intensity), electro-oxidation (same reactor without using the Fe(II) loaded resin) and electro-Fenton using cathode-to-anode flow and anode-to-cathode flow directions. As shown in Fig. 6a, while the TOC values reflect negligible removal by adsorption, the electrochemical oxidation process results in a value of 28.92%. As expected, TOC decrease was largely improved by (after 30 min of electrolysis) the electro-Fenton process using either the anode-to-cathode set-up (45.5%), or the cathode-to-anode arrangement (57.9%). This observation not only confirms that the •OH radical species is generated by Eq. (3), playing the most important role in the mineralization of the AMX, but also that the cathode-to-anode configuration allows to obtain the higher yields. Fig. 6b on the other hand, shows the mineralization efficiency of the cathode-to-anode configured electro-Fenton process for real sanitary wastewater, which was previously contaminated with AMX as described in the experimental section. Using this complex effluent matrix, a 38.6% of mineralization was achieved after 30 min of reaction. The lower effectiveness of the process using this solution is probably related to the presence of soluble organic matter that not only inhibits the electro-generation of H_2O_2, but also promotes competitive reactions. As it can be noted from the experimental data, the quasi-steady state was reached after 3 mean hydraulic residence times.

It is interesting to compare the AMX mineralization data obtained in this study with reports using electro-Fenton process. In this way, Kadji et al. (2021) obtained 74% of AMX mineralization after 180 min of electrolysis, with an initial AMX concentration of 0.082 mM; however, this value was reduced to 39% at 0.164 mM of AMX due to a competitive consumption of oxidizing •OH radicals between AMX and the by-products

formed during experiments (Kadji et al. 2021). On the other hand, Garza-Campos et al. (2018) obtained 55% of AMX mineralization after 240 min of treatment using BDD anode and an air diffusion mesoporous carbon cathode (Garza-Campos et al. 2018). Furthermore, since in the electro-Fenton process the •OH is determined as the dominant oxidant, the acute toxicity of the solution of the water after the treatment was reduced in 50% using *Daphnia magna* as a biological indicator (Zhang et al. 2021).

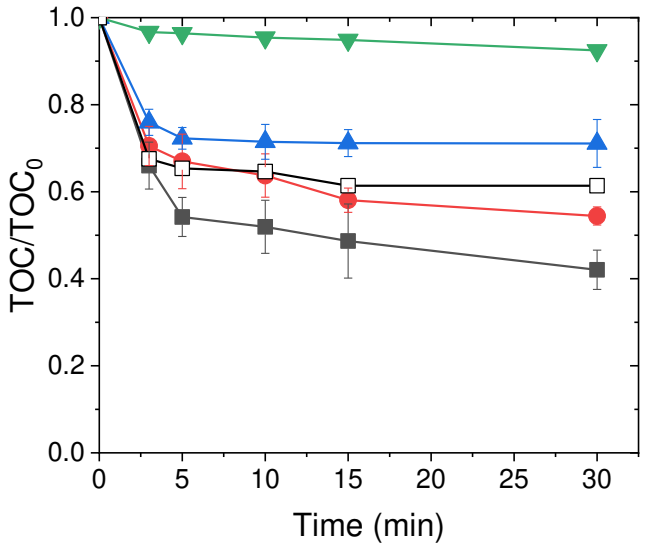

Fig. 6. TOC removal for AMX degradation assays using a synthetic solution: black ■ electro-Fenton process, cathode-to-anode flow configuration with oxygen saturation, red •: electro-Fenton process, anode-to-cathode flow arrangement with oxygen saturation, blue ▲ electrochemical oxidation process, cathode-to-anode flow set-up with oxygen saturation, green ▼: adsorption (without current). Using real sanitary wastewater: empty black ■ electro-Fenton process, cathode-to-anode flow arrangement with oxygen saturation. 300 mA, pH 7, 500 mL min^{-1} recirculation flow rate.

The concentration of the NO_3^- was also determined as evidence of the degradation of the antibiotic by means of the electro-Fenton process arranged in the cathode-to-anode configuration. Fig. 7a shows the NO_3^- concentration on time, and it can be noted that the ion concentration increases with increasing treatment time up to a concentration of 3.6 mg L^{-1}. The presence of NO_3^- is explained by the mineralization reaction of AMX (Eq. 12), which produces NH_4^+ that in turn, when interacting with •OH radicals, generates NO_2^- (Eq. 13) and eventually NO_3^- (Eq. 14).

$$C_{16}H_{19}N_3O_5S + 31H_2O \rightarrow 16CO_2 + 3NH_4^+ + SO_4^{2-} + 69H^+ + 70e^- \quad (15)$$

448 $$2^{\bullet}OH + NH_4^+ \rightarrow NO_2^- + 6H^+ + 6e^- \quad (16)$$

449 $$2^{\bullet}OH + NO_2^- \rightarrow NO_3^- + H_2O + e^- \quad (17)$$

450 Fig. 8 depicts a diagram of the pathways that takes place within the flow-through electro-
451 Fenton reactor for the mineralization of the AMX. To achieve the abovementioned, it is
452 necessary the reduction of the dissolved oxygen at the carbon felt cathode to promote
453 H_2O_2 and the concomitant production of $^{\bullet}OH$ by the presence of the Fe(II) washed from
454 the iron loaded resin placed in the C*1* compartment of the reactor to finally obtain CO_2,
455 H_2O and inorganic ions.

456

457 **Disinfection assays**

458 In order to test the efficiency of the process in the inactivation of fecal coliforms, real
459 sanitary wastewater treated by an anaerobic biodigester and anoxic-aerobic bioreactor
460 was used. Under the optimal conditions of the electro-Fenton reactor, Fig. 7b shows that
461 after 5 min of electrolysis, it was possible to reduce the concentration of the fecal coliform
462 from 24 000 MPN 100 mL^{-1} to 2400 NMP 100 mL^{-1} and this value was maintained after
463 30 min of treatment; which means an efficiency of inactivation of pathogens of 90%. On
464 the other hand, when the water passed through the system in the absence of current,
465 there was no decrease in fecal coliforms after 5 min and after 30 min a value of 11 000
466 MPN 100 mL^{-1} was obtained; indicating that under these conditions, around 50% of
467 coliforms can be retained in reaction system.

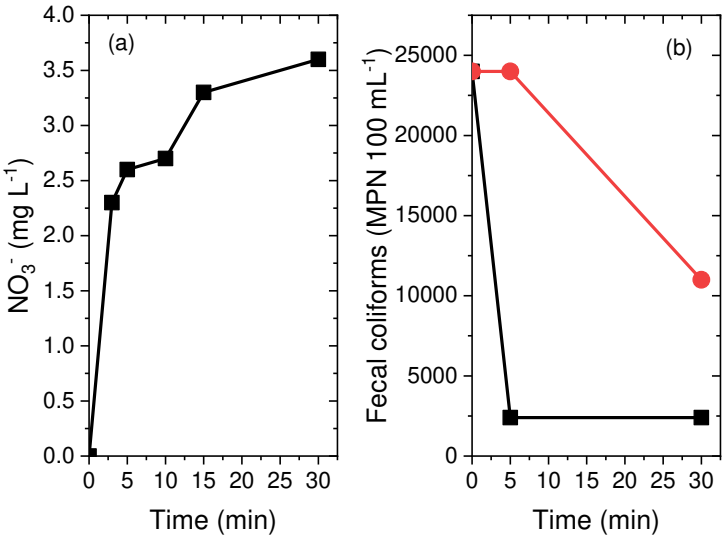

468

Fig. 7. (a) NO_3^- from AMX degradation and (b) fecal coliforms concentration *vs* time in real wastewater. Black ■: electro-Fenton process in cathode-to-anode configuration, red •: adsorption process.

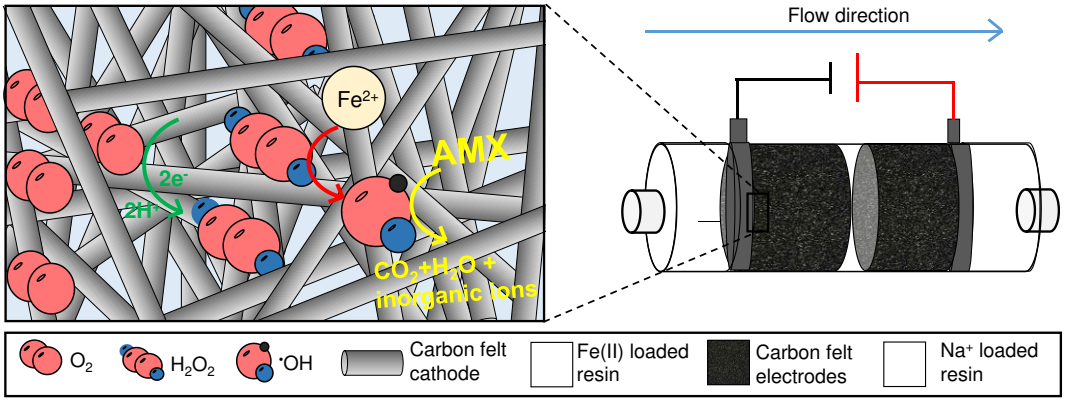

Fig. 8. Schematic diagram of AMX mineralization within the proposed cylindrical flow-through electro-Fenton reactor using carbon felt electrodes.

Conclusions

The performance of a cylindrical flow-through electro-Fenton reactor using carbon felt electrodes was evaluated. An experimental design methodology was applied to evaluate the effects of four independent variables and to determine the best experimental conditions. Among the studied factors current and treatment time were the most meaningful parameters. The best operational parameters were found to be: current of 300 mA during 30 min, 500 mL min^{-1} of recirculation flow rate, with the electrodes placed in the middle of the reactor and at cathode-to-anode flow direction achieving a H_2O_2 concentration of 16.1 mg L^{-1} and energy consumption of 3.21 kWh m^{-3}. Under these conditions, the system allows to obtain a ·OH concentration of 3.11 µM, a AMX mineralization efficiency of 57.9% and a fecal coliforms inactivation of 90%. The proposed reactor appears to be a promising modular technology that can be used as tertiary treatment to remove contaminants of emerging concern and to the disinfection of wastewaters.

References

Aquino JM, Rocha-Filho RC, Rodrigo MA, et al (2013) Electrochemical degradation of the Reactive Red 141 dye using a boron-doped diamond anode. Water Air Soil Pollut 224:. https://doi.org/10.1007/s11270-012-1397-9

aus der Beek T, Weber FA, Bergmann A, et al (2016) Pharmaceuticals in the environment-Global occurrences and perspectives. Environ Toxicol Chem 35:823–835. https://doi.org/10.1002/etc.3339

Brillas E (2020) A review on the photoelectro-Fenton process as efficient electrochemical advanced oxidation for wastewater remediation. Treatment with UV light, sunlight, and coupling with conventional and other photo-assisted advanced technologies. Chemosphere 250:. https://doi.org/10.1016/j.chemosphere.2020.126198

Brillas E, Martínez-Huitle CA (2015) Decontamination of wastewaters containing synthetic organic dyes by electrochemical methods. An updated review. Appl Catal B Environ 166–167:603–643. https://doi.org/10.1016/j.apcatb.2014.11.016

Brillas E, Sirés I, Oturan MA (2009) Electro-fenton process and related electrochemical technologies based on fenton's reaction chemistry. Chem Rev 109:6570–6631. https://doi.org/10.1021/cr900136g

Carrera-Cevallos JV, Prato-Garcia D, Espinoza-Montero PJ, Vasquez-Medrano R (2021) Electro-oxidation of a Commercial Formulation of Glyphosate on Boron-Doped Diamond Electrodes in a Pre-pilot-Scale Single-Compartment Cell. Water Air Soil Pollut 232:. https://doi.org/10.1007/s11270-020-04941-z

Castillo-Monroy J, Godínez LA, Robles I, Estrada-Vargas A (2020) Study of a coupled adsorption/electro-oxidation process as a tertiary treatment for tequila industry wastewater. Environ Sci Pollut Res. https://doi.org/10.1007/s11356-020-11031-4

Chai Y, Qin P, Wu Z, et al (2021) A coupled system of flow-through electro-Fenton and electrosorption processes for the efficient treatment of high-salinity organic wastewater. Sep Purif Technol 267:. https://doi.org/10.1016/j.seppur.2021.118683

Commission Implementing Decision (EU) 2015/495 of 20 (2015) Watch list of substances for Union-wide monitoring in the field of water policy pursuant to Directive 2008/105/EC of the European Parliament and of the Council

Comninellis C (1994) Electrocatalysis in the electrochemical conversion/combustion of organic pollutants for waste water treatment. Electrochim Acta 39:1857–1862.

https://doi.org/10.1016/0013-4686(94)85175-1

Daghrir R, Drogui P, El Khakani MA (2013) Photoelectrocatalytic oxidation of chlortetracycline using Ti/TiO_2 photo-anode with simultaneous H_2O_2 production. Electrochim Acta 87:18–31. https://doi.org/10.1016/j.electacta.2012.09.020

Daghrir R, Drogui P, Tshibangu J, et al (2014) Electrochemical treatment of domestic wastewater using boron-doped diamond and nanostructured amorphous carbon electrodes. Environ Sci Pollut Res 21:6578–6589. https://doi.org/10.1007/s11356-014-2558-8

de Matos DB, Barbosa MPR, Leite OM, et al (2020) Characterization of a tubular electrochemical reactor for the degradation of the commercial diuron herbicide. Environ Technol (United Kingdom) 41:1307–1321. https://doi.org/10.1080/09593330.2018.1531941

Droguett C, Salazar R, Brillas E, et al (2020) Treatment of antibiotic cephalexin by heterogeneous electrochemical Fenton-based processes using chalcopyrite as sustainable catalyst. Sci Total Environ 740:. https://doi.org/10.1016/j.scitotenv.2020.140154

Fu J, Zhao Y, Wu Q (2007) Optimising photoelectrocatalytic oxidation of fulvic acid using response surface methodology. J Hazard Mater 144:499–505. https://doi.org/10.1016/j.jhazmat.2006.10.071

García-Espinoza JD, Gortáres-Moroyoqui P, Orta-Ledesma MT, et al (2016) Electrochemical removal of carbamazepine in water with Ti/PbO_2 cylindrical mesh anode. Water Sci Technol 73:1155–1165. https://doi.org/10.2166/wst.2015.591

García-Espinoza JD, Mijaylova-Nacheva P, Avilés-Flores M (2018) Electrochemical carbamazepine degradation: Effect of the generated active chlorine, transformation pathways and toxicity. Chemosphere 192:142–151. https://doi.org/10.1016/j.chemosphere.2017.10.147

García-Espinoza JD, Robles I, Gil V, et al (2019) Electrochemical degradation of triclosan in aqueous solution. A study of the performance of an electro-Fenton reactor. J Environ Chem Eng 7:. https://doi.org/10.1016/j.jece.2019.103228

Garcia-Segura S, Qu X, Alvarez PJJ, et al (2020) Opportunities for nanotechnology to enhance electrochemical treatment of pollutants in potable water and industrial wastewater-a perspective. Environ Sci Nano 7:2178–2194. https://doi.org/10.1039/d0en00194e

556 Garza-Campos B, Morales-Acosta D, Hernández-Ramírez A, et al (2018) Air diffusion
557 electrodes based on synthetized mesoporous carbon for application in amoxicillin
558 degradation by electro-Fenton and solar photo electro-Fenton. Electrochim Acta
559 269:232–240. https://doi.org/10.1016/j.electacta.2018.02.139

560 Haoran P, Valérie L, Etienne P, Gilles H (2013) The influence of porous structure and
561 biofilm on the hydrodynamics of two types of trickle filters. Chem Eng J 231:163–
562 171. https://doi.org/10.1016/j.cej.2013.06.115

563 Heck KN, Garcia-Segura S, Westerhoff P, Wong MS (2019) Catalytic Converters for
564 Water Treatment. Acc Chem Res 52:906–915.
565 https://doi.org/10.1021/acs.accounts.8b00642

566 Jiao Y, Ma L, Tian Y, Zhou M (2020) A flow-through electro-Fenton process using
567 modified activated carbon fiber cathode for orange II removal. Chemosphere 252:.
568 https://doi.org/10.1016/j.chemosphere.2020.126483

569 Jones OAH, Voulvoulis N, Lester JN (2002) Aquatic environmental assessment of the
570 top 25 English prescription pharmaceuticals. Water Res 36:5013–5022.
571 https://doi.org/10.1016/S0043-1354(02)00227-0

572 Kadji H, Yahiaoui I, Garti Z, et al (2021) Kinetic degradation of amoxicillin by using the
573 electro-Fenton process in the presence of a graphite rods from used batteries.
574 Chinese J Chem Eng. https://doi.org/10.1016/j.cjche.2020.08.032

575 Komtchou S, Dirany A, Drogui P, Bermond A (2015) Removal of carbamazepine from
576 spiked municipal wastewater using electro-Fenton process. Environ Sci Pollut Res
577 22:11513–11525. https://doi.org/10.1007/s11356-015-4345-6

578 Ma P, Ma H, Galia A, et al (2019) Reduction of oxygen to H_2O_2 at carbon felt cathode
579 in undivided cells. Effect of the ratio between the anode and the cathode surfaces
580 and of other operative parameters. Sep Purif Technol 208:116–122.
581 https://doi.org/10.1016/j.seppur.2018.04.062

582 Martin-Dominguez A, Tzatchkov VG, Martin-Dominguez IR, Lawler DF (2005) An
583 enhanced tanks-in-series model for interpretation of tracer tests. J Water Supply
584 Res Technol - AQUA 54:435–448. https://doi.org/10.2166/aqua.2005.0041

585 Mompelat S, Le Bot B, Thomas O (2009) Occurrence and fate of pharmaceutical
586 products and by-products, from resource to drinking water. Environ Int 35:803–
587 814. https://doi.org/10.1016/j.envint.2008.10.008

588 Monteil H, Pechaud Y, Oturan N, et al (2021) Pilot scale continuous reactor for water

589 treatment by electrochemical advanced oxidation processes: Development of a
590 new hydrodynamic/reactive combined model. Chem Eng J 404:.
591 https://doi.org/10.1016/j.cej.2020.127048

592 Murillo-Sierra JC, Sirés I, Brillas E, et al (2018) Advanced oxidation of real
593 sulfamethoxazole + trimethoprim formulations using different anodes and
594 electrolytes. Chemosphere 192:225–233.
595 https://doi.org/10.1016/j.chemosphere.2017.10.136

596 Panizza M, Oturan MA (2011) Degradation of Alizarin Red by electro-Fenton process
597 using a graphite-felt cathode. Electrochim Acta 56:7084–7087.
598 https://doi.org/10.1016/j.electacta.2011.05.105

599 Petrucci E, Da Pozzo A, Di Palma L (2016) On the ability to electrogenerate hydrogen
600 peroxide and to regenerate ferrous ions of three selected carbon-based cathodes
601 for electro-Fenton processes. Chem Eng J 283:750–758.
602 https://doi.org/10.1016/j.cej.2015.08.030

603 Puga A, Moreira MM, Figueiredo SA, et al (2021) Electro-Fenton degradation of a
604 ternary pharmaceutical mixture and its application in the regeneration of spent
605 biochar. J Electroanal Chem 886:. https://doi.org/10.1016/j.jelechem.2021.115135

606 Ren G, Zhou M, Liu M, et al (2016) A novel vertical-flow electro-Fenton reactor for
607 organic wastewater treatment. Chem Eng J 298:55–67.
608 https://doi.org/10.1016/j.cej.2016.04.011

609 Ren G, Zhou M, Zhang Q, et al (2020) A novel stacked flow-through electro-Fenton
610 reactor as decentralized system for the simultaneous removal of pollutants (COD,
611 NH_3-N and TP) and disinfection from domestic sewage containing chloride ions.
612 Chem Eng J 387:. https://doi.org/10.1016/j.cej.2020.124037

613 Robles I, Becerra E, Barrios JA, et al (2020) Inactivation of helminth eggs in an electro-
614 Fenton reactor: Towards full electrochemical disinfection of human waste using
615 activated carbon. Chemosphere 250:.
616 https://doi.org/10.1016/j.chemosphere.2020.126260

617 Salmerón I, Oller I, Plakas K V., Malato S (2021) Carbon-based cathodes degradation
618 during electro-Fenton treatment at pilot scale: Changes in H_2O_2 electrogeneration.
619 Chemosphere 275:. https://doi.org/10.1016/j.chemosphere.2021.129962

620 Tokumura M, Morito R, Hatayama R, Kawase Y (2011) Iron redox cycling in hydroxyl
621 radical generation during the photo-Fenton oxidative degradation: Dynamic

622 change of hydroxyl radical concentration. Appl Catal B Environ 106:565–576.
623 https://doi.org/10.1016/j.apcatb.2011.06.017

624 Yu F, Chen Y, Pan Y, et al (2020) A cost-effective production of hydrogen peroxide via
625 improved mass transfer of oxygen for electro-Fenton process using the vertical
626 flow reactor. Sep Purif Technol 241:. https://doi.org/10.1016/j.seppur.2020.116695

627 Zaviska F, Drogui P, Blais JF, et al (2011) Experimental design methodology applied to
628 electrochemical oxidation of the herbicide atrazine using Ti/IrO2 and Ti/SnO2
629 circular anode electrodes. J Hazard Mater 185:1499–1507.
630 https://doi.org/10.1016/j.jhazmat.2010.10.075

631 Zaviska F, Drogui P, Pablo G (2012) Statistical optimization of active chlorine
632 production from a synthetic saline effluent by electrolysis. Desalination 296:16–23.
633 https://doi.org/10.1016/j.desal.2012.03.023

634 Zhang J, Zheng C, Dai Y, et al (2021) Efficient degradation of amoxicillin by scaled-up
635 electro-Fenton process: Attenuation of toxicity and decomposition mechanism.
636 Electrochim Acta 381:. https://doi.org/10.1016/j.electacta.2021.138274

637 Zhou L, Zhou M, Hu Z, et al (2014) Chemically modified graphite felt as an efficient
638 cathode in electro-Fenton for p-nitrophenol degradation. Electrochim Acta
639 140:376–383. https://doi.org/10.1016/j.electacta.2014.04.090

640 Zhou M, Ren G, Ma L, et al (2017) Cost-effective flow-through reactor in electro-
641 Fenton. In: Handbook of Environmental Chemistry. pp 241–261

642 Zhou M, Tan Q, Wang Q, et al (2012) Degradation of organics in reverse osmosis
643 concentrate by electro-Fenton process. J Hazard Mater 215–216:287–293.
644 https://doi.org/10.1016/j.jhazmat.2012.02.070

Declarations:

Ethics approval and consent to participate

Not applicable.

Consent for publication

Not applicable.

Availability of data and materials

Not applicable.

Competing interests

The authors declare no competing interests and that there are no conflicts of interests regarding the publication of this work.

Funding

- Mexican Council for Science and Technology; CONACYT (Grant No. PENTA2019-1-303758 and CB-2016-01-285309).
- Ministry for Education, Science, Technology and Innovation of CDMX (SECTEI/259/2019).
- Bill and Melinda Gates Foundation (Grant No. OPP1156657).

Authors' contributions

- Josué Daniel García-Espinoza: Investigation, Validation, Formal analysis.
- Irma Robles: Investigation, Methodology, Formal analysis.
- Alfonso Durán-Moreno: Investigation, Formal analysis, Supervision
- Luis A. Godínez: Conceptualization, Writing- Reviewing and Editing, Project administration, Funding acquisition.

673

674 **Acknowledgements**

675 The authors express their gratitude to the Mexican Council for Science and Technology;
676 CONACYT (Grant No. PENTA2019-1-303758 and CB-2016-01-285309), the Ministry for
677 Education, Science, Technology and Innovation of CDMX (SECTEI/259/2019) and to the
678 Bill and Melinda Gates Foundation (Grant No. OPP1156657), for their financial support
679 of this work.

Supplementary Files

This is a list of supplementary files associated with this preprint. Click to download.

- 2021ESPRSM.docx